P3-29

On MARFE stability and movement in an ELMy H-mode Discharge in NSTX

F. Kelly[a], R. Maqueda[b], R. Maingi[c], J. Menard[a], B. LeBlanc[a], R. Bell[a], S. Paul[a]

[a] *Princeton Plasma Physics Laboratory, Princeton, NJ USA*

[b] *Nova Photonics, Princeton, NJ USA*

[c] Oak Ridge National Laboratory, Oak Ridge, TN USA

Abstract

The results of a comparison of MARFE theory with experiment in the National Spherical Torus Experiment are presented. Using a fast-framing camera, MARFEs are observed to move and to interact with ELMs during the ELM cycle. A basic MARFE theory was applied to NSTX Thomson scattering and CHERS data. MARFE theory generally correlated with experiment, but timing restrictions, uncertainty in the location of the separatrix location and lack of spatial resolution constrained the analysis. The movements of MARFEs are interpreted to result from the combined effects of the E × B and diamagnetic drifts.

1. Introduction

The maximum plasma density attainable before the occurrence of a change in the discharge performance is a fundamental operational boundary for fusion devices [1]. Multifaceted Asymmetric Radiation From the Edge (MARFE) is a poloidally and radially localized but toroidal symmetric region of high density, low temperature, strongly radiating plasma that is frequently observed at the high field side (HFS) of toroidal confinement devices when the edge density increases beyond a certain limit. Edge Localized Modes (ELMs) are periodic bursts of particles and power released by filaments aligned with the magnetic field from the low field side (LFS) of toroidal confinement devices during the high confinement mode (H-mode) of operation which characteristically form large density pedestals with steep gradients inside the low field edge. The National Spherical Torus Experiment (NSTX) is unique among toroidal confinement devices in that MARFEs and ELMs can coexist within the same H-mode discharge [2]. In this paper we present the results of an analysis of MARFE stability and movement in NSTX.

NSTX operates using up to 7 MW of neutral beam injection at low aspect ratio with R = 0.85 m and a = 0.65 m ($R/a \approx 1.3$), elongations up to 2.8, plasma currents up to 1.5 MA, B_T = 0.3 to 0.55 T and triangularities up to 0.8 [3-6]. Plasma facing components are protected from the plasma by a combination of graphite and carbon fiber composite tiles. The dominant impurity is carbon. This experiment was NSTX shot 117125 conducted with plasma current I_p = 0.9 MA and on-axis toroidal field B_t = 0.45 T, in a double null discharge shape with elongation $\kappa \sim 2.4$, triangularity $\delta \sim 0.7$, and the ion grad-B drift toward the lower X-point.

Observations of MARFE and ELMs with a fast-framing digital camera and discussion of measurements of the plasma parameters is presented in Section 2. Basic MARFE stability theory is reviewed and applied to NSTX measurements in Section 3. A model for MARFE movement is presented in Section 4. Conclusions are presented in Section 5.

2. Experimental observations and measurements

The rapidly evolving MARFE and ELM structures were observed in NSTX using a Phantom 7.1 fast-framing digital camera [2]. A wide-angle, fish eye elevation view of the center column together with upper and lower divertor regions were obtained for NSTX shot 117125 with a D_α-line bandpass filter. A highly-radiating, poloidally and toroidally localized region of cold, dense plasma (plasmoid) is seen to spiral helically upward around the center column, approximately following the magnetic field pitch (see Fig. 4a of Ref. 2). This plasmoid is the result of Type III ELM activity in which heat is transported along the field lines from the ELM filament on the LFS to a ring MARFE that encompasses the center stack. The parallel heat flux partially burns through the ring MARFE and the remnant plasmoid moves away from the lower divertor following the local magnetic field line at a speed of ~ 15 km/s. The motion of the plasmoid stagnates, typically above the midplane, as the ELM filament has released its excess pressure. The ring MARFE reforms as it moves downward towards the lower divertor. Several cycles of this MARFE/ELM interaction are shown in Fig. 2. The downward velocity of the ring MARFE is seen to be slowing from 1.77 km/s at 658 ms, to 1.54 km/s at 660 ms, to 1.49 km/s at 661.5 ms, to 1.46 km/s at 663 ms. By 665 ms, the downward velocity has slowed to 0.94 km/s and MARFE has thickened substantially

and then begins to move upward just before a Type I ELM occurs. The variation in MARFE velocity and size is due to changing edge parameters.

The kinetic profile diagnostics used to measure the edge parameters include Thomson scattering (TS) and charge exchange recombination spectroscopy (CHERS). The Thomson scattering diagnostic provides measurements of the electron density and temperature profiles along the major radius, $n_e(R,t)$ and $T_e(R,t)$, using two lasers with a time resolution of 16.6667 ms (2 × 30 Hz) and utilizes 30 spatial channels. CHERS provides measurements of the C^{6+} ion density and temperature, and toroidal velocity profiles, $n_i(R,t)$, $T_i(R,t)$ and $v_\Phi(R,t)$ of the intrinsic carbon impurity with a time resolution of 10 ms and utilizes 51 spatial channels. The TS measurement is essentially instantaneous while the CHERS measurement is integrated over ~8.2 ms, buffered in ~1.8 ms and centered in the 10 ms time interval. Since the plasma profiles are dynamically evolving, the MARFE stability analysis is restricted to times where the difference between the TS and CHERS sample time is a minimum, that is where $| t_{TS} - t_{CHERS} | < 1.5$ ms. This gives the best chance of obtaining consistent data to use in our comparison with theory.

The spatial resolution of the TS measurement is not sufficient to resolve the electron temperature and density in the NSTX plasma edge where steep gradient exist in H-mode. Thus, we depend on interpolation algorithms to obtain estimates from the TS data. An additional problem is that equilibrium codes EFIT and LRDFIT do not accurately determine the location of the separatrix. It is believed, however, that the HFS separatrix is more accurately determined since the magnetic field sensors are located closer to the plasma edge on the HFS. Therefore, we adjust the TS and CHERS profiles using the following procedure

developed by one of the authors (RM). We assume the electron temperature is constant on the poloidal flux surface and the HFS separatrix is accurately located. In ψ_N-space, the LFS T_e data points are shifted visually until the data points appear to form a smooth profile with a couple of T_e data points from the HFS. This ψ_N-space shift is then used to adjust the TS and CHERS data that satisfy the timing requirement stated above. The carbon impurity fraction, $f_C = n_C/n_e$, was estimated from the CHERS C6+ density and TS electron density. The carbon fraction was observed to generally decrease from the pedestal to the separatrix due recombination into lower charge states. It was assumed that carbon fraction was usually constant in the edge, therefore the maximum f_C value in the edge was used.

The observations and measurements using the procedures described above with LRDFIT04 are summarized in Table 1. Occasionally, e.g. at 527 ms, the assumption that the HFS separatrix is accurately determined by the equilibrium code seemed to be invalid.

3. Basic MARFE stability theory

MARFEs were first observed in Alcator-C and attributed to a radiative thermal instability in the parallel energy balance by Lipschultz, et al. [7]. Stringer [8] and Neuhauser [9] concluded that parallel conduction controls the onset of thermal instability. Drake [10] identified the MARFE as a radiative condensation instability with astrophysical counterparts. Wesson and Hender [11] observed that the most unstable mode varies as cos θ with wave number k = 1/qR, where θ is the poloidal angle, q is the safety factor and R is the major radius. The Wesson and Hender model used the coronal radiation model $L_z(T)$ of Post, et al. [12]. This was modified by Mahdavi, et al. [13] and Maingi and Mahdavi [14] who

incorporated the non-equilibrium radiation effect of neutrals in a uniform edge distribution to obtain an equation that is equivalent to

$$n_{marfe} = \sqrt{\frac{\left(\kappa_0 / Z_{eff}\right) T^{1/2} / (qR)^2}{-\sum_z f_z \frac{\partial}{\partial T}\left(\frac{L_z(T, f_0)}{T^2}\right)}} \qquad (1)$$

the MARFE density limit, where $\kappa_{\|} = \left(\kappa_0 / Z_{eff}\right) T^{5/2}$ is the Spitzer parallel conductivity, $f_z = n_z/n_e$ is the impurity fraction and $f_0 = n_0/n_e$ is the neutral fraction. Defining the MARFE Index, MI = n_{exp}/n_{marfe}, the calculation of MARFE stability for NSTX discharge 117125 using Eq. (1) is shown in Fig. 3 assuming $f_0 = 10^{-3}$ and the Thomson and CHERS data in Table 1. Figure 3 shows the trend of MI to tend toward 1 when a MARFE is born or already exists. The uncertainty in the measured parameters is rather large.

4. MARFE movement

Chankin [15] found that the growth rate of the MARFE instability is unaffected by the poloidal E × B drift. Chankin's analysis found that the only consequence of poloidal E × B rotation was that the poloidal rotation of the MARFE was at the same velocity as the background plasma. In H-mode plasmas, the radial electric field just inside the separatrix is negative. Thus, in NSTX shot 117125 the movement of the MARFE should be directed downward, however, at 377 ms the MARFE was observed moving upward. Another possible explanation is offered by Tokar [16]. The MARFE moves because one of the MARFE borders is cooled and the other heated by drift diamagnetic heat flows, due to their pressure dependence. Here, we make the additional observation that the motion of the MARFE due to diamagnetic heat flows will be relative to the velocity of the background plasma.

We use non-stationary equations for heat transport taking into account heat flows both across and along magnetic surfaces. Due to the Shafranov shift of magnetic flux surfaces, the temperature and density gradients are largest at the LFS of the discharge. These gradients drive instabilities which cause the heat loss though the edge boundary, q_b, to be poloidally asymmetric. We assume the θ dependence of q_b to be of the form $q_b = \overline{q}_b(1-\beta\cos\theta)$ where $\overline{q}_b = Q_b / A_p$, Q_b is the net power transported to the periphery, A_p is the area of the peripheral magnetic surface, β is the asymmetry factor for power transport and $\theta = 0$ at the HFS midplane. In NSTX between 70% and 80% of the power is transported through the LFS. We assume $\overline{q}_{LFS}/\overline{q}_b = 0.75$ and thus $\beta = \pi/4$ and $\overline{q}_{HFS} = 0.25\,\overline{q}_b$.

Defining $\alpha_{\nabla T} = \nabla_r T_i / \nabla_r T_e$, $\alpha_T = T_i / T_e$ and taking $\frac{\partial T}{\partial r} = -\frac{q_b}{\kappa_r}$, we may write $q_{d,\perp} = \frac{5}{2}\frac{P}{eB}\frac{q_b}{\kappa_\perp}\left(1-\alpha_{\nabla T}\alpha_T\right)$. Taking the terms describing the dependencies of the pressure on t and θ, and assuming the other terms constant, we write the heat equation as:

$$\frac{3}{2}\frac{\partial P}{\partial t} + \frac{5}{2}\left(1-\alpha_{\nabla T}\alpha_T\right)\frac{q_b}{eB\kappa_r a}\frac{\partial P}{\partial \vartheta} = C \qquad (2)$$

where $P = n(T_i + T_e)$ and a is the minor radius. We take perturbations of P of the form $\tilde{P} \propto \exp\left(V_{\vartheta d}\,t - a\vartheta\right)$ and estimate the poloidal diamagnetic drift velocity to be

$$V_{\theta d} = \frac{5}{3}\frac{q_b}{eB\kappa_r}\left(1-\alpha_{\nabla T}\alpha_T\right) \qquad (3)$$

Using Thomson measurements of n_e and T_e and CHERS measurements of T_i on the low field side (LFS), we estimate for shot 117125 at 377 ms $\alpha_{\nabla T} = 3.9$, $\alpha_T = 9.4$ and $V_{\theta d}$ =

1.0 km/s upward. At 660 ms, we estimate $\alpha_{\nabla T} = 0.85$, $\alpha_T = 8.2$ and $V_{\theta d} = 3.6$ km/s upward. We estimate from the fast-framing camera images the experimental poloidal velocity of the MARFE to be 1.88 km/s upward at 377 ms and 1.54 km/s downward at 660 ms. If the total poloidal MARFE velocity is the poloidal diamagnetic drift velocity relative to the background plasma velocity, then the E × B drift is 1.7 km/s downward and $E_r = -3.3$ kV/m at 377 ms and 2.6 km/s downward and $E_r = -4.6$ kV/m at 660 ms. Similar values of the radial electric field during H-mode were measured by Biewer [17] in NSTX shot 110077, which was double-null, D fueled, $B_T(0) = -0.45$ T, $I_p = 1$ MA and P_{NBI} up to 5.1 MW. Due to the uncertainties in measurements and many assumptions made in calculation, these estimates are themselves uncertain. However, the calculation illustrates that reasonable assumptions lead to values that are the correct order of magnitude.

5. Conclusions

The MARFE density limit predicted by basic MARFE theory, roughly agrees with NSTX experimental measurement, but uncertainties in the data limit the comparison. The theory of Chankin [15] that the E × B drift controls MARFE movement is not consistent with observation in NSTX. Tokar [16] proposed a theory that the MARFE moves because one of the MARFE borders is cooled and the other heated by drift diamagnetic heat flows, which is also not consistent with observations in NSTX. However, if the poloidal movement of the MARFE is the sum of the E × B drift and diamagnetic heat flow driven motion, then MARFE movement in NSTX may be explained with an E_r of the right order of magnitude. In another paper, we will examine whether diamagnetic drift can describe the movement of Type V ELMs or the shearing of convective cells responsible for anomalous transport.

Acknowledgements

Research sponsored in part by U.S. D.o.E. contracts DE-FG02-04ER54767, DE-AC02-76CH03073 and DE-AC05-00OR22725.

References

[1] M. Greenwald, Plasma Phys. Controlled Fusion 44 (2002) R27.

[2] R.J. Maqueda, R. Maingi, K. Tritz, et al., J. Nucl. Mater. 363-365 (2007) 1000.

[3] B.P. LeBlanc, R.E. Bell, S.M. Kaye, et al., Nucl. Fusion 44 (2004) 513.

[4] S.M. Kaye, M.G. Bell, R.E. Bell, et al., Nucl. Fusion 45 (2005) S168.

[5] M.G. Bell, R.E. Bell, D.A. Gates, et al., Nucl. Fusion 46 (2006) S565.

[6] J.E. Menard, M.G. Bell, R.E. Bell, et al., Nucl. Fusion 47 (2007) S645.

[7] B. Lipschultz, B. LaBombard, E.S. Marmar, et al., Nucl. Fusion 24 (1984) 977.

[8] T.E. Stringer, in *Proc. 12 European Conf. on Controlled Fusion and Plasma Physics,* Budapest, Hungary, 1985 (European Physical Society, Budapest, 1985), part I, p. 86.

[9] J. Neuhauser, W. Schneider and R.O. Wunderlich, Nucl. Fusion 26 (1986) 1679.

[10] J.F. Drake, Phys. Fluids 30 (1987) 2429.

[11] J.A. Wesson and T.C. Hender, Nucl. Fusion 33 (1993) 1019.

[12] D.E. Post, et al., At. Data Nucl. Data Tables 20 (1977) 397.

[13] M.A. Mahdavi, et al., in *Proc. 24th European Conf. Controlled Fusion and Plasma Physics*, Berchtesgaden, Germany, 1997, Vol. 21A, p. 1113, (European Physical Society,1997).

[14] R. Maingi and M.A. Mahdavi, Fusion Sci. and Technol. 48 (2005) 1117.

[15] A.V. Chankin, Phys. Plasma 11 (2004) 1484.

[16] M. Z. Tokar, Contrib. Plasma Phys. 32 (1992) 341.

[17] Biewer, et al., Rev. Sci. Inst. 75 (2004) 650.

Figure captions

Table 1: MARFE observations for NSTX discharge 117125 at the Thomson Scattering times and the data used in the MARFE stability calculation if $| t_{TS} - t_{CHERS} | < 1.5$ ms.

Fig. 1: MARFE/ELM cycles in NSTX discharge 117125: (a) "streak" image showing the plasmoid spiral upward, stagnate, reform a MARFE which moves downward until an ELM partially burns though the MARFE leaving a plasmoid as a remnant to begin a new cycle and (b) the D_α light signal from the lower divertor.

Fig. 2: Cases observed in NSTX discharge 117125 with case numbers assigned. The center image is nearest the TS time given, the left image -72.5 μs earlier and the right image +72.5 μs later.

Fig. 3: Case numbers and MARFE Index at the sample times where $| t_{TS} - t_{CHERS} | < 1.5$ ms.

Table 1:

TS time [s]	Condition	CHERS time	T_e [eV]	n_e [m-3]	f_C [%]
0.326662	no marfe	0.32525	59	2.0E19	7.2
0.343345	no marfe	0.33525			
0.359992	no marfe	0.35525			
0.376685	upward move	0.37525	35	2.2E19	6.4
0.393332	no marfe	0.38525			
0.410015	no marfe	0.40525			
0.426662	no marfe	0.42525	35	1.6E19	5.2
0.443345	no marfe	0.43525			
0.459992	no marfe	0.45525			
0.476685	birth	0.47525	34	2.9E19	6.2
0.493322	stagnation	0.48525			
0.510025	stagnation	0.50525			
0.526662	no marfe	0.52525	134	3.2E19	4.8
0.543345	birth	0.53525			
0.559992	no marfe	0.55525			
0.576685	no marfe	0.57525	39	2.1E19	6.7
0.593332	birth	0.58525			
0.610025	no marfe	0.60525			
0.626662	burn	0.62525	35	1.8E19	10.7
0.643355	stagnation	0.63525			
0.660002	move down	0.65525			
0.676685	stable at top	0.67525	37	2.1E19	4.4
0.693332	no marfe	0.68525			
0.710015	birth	0.70525			
0.726662	birth	0.72525	36	2.1E19	4.8
0.743355	no marfe	0.73525			
0.759992	no marfe	0.75525			
0.776685	no marfe	0.77525	74	2.9E19	5.9
0.793332	no marfe	0.78525			
0.810015	stagnation	0.80525			

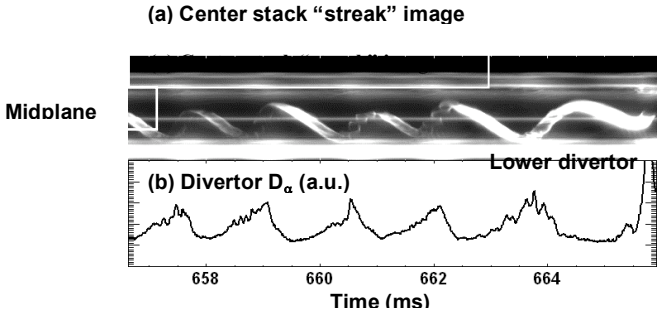
(a) Center stack "streak" image
Midplane
Lower divertor
(b) Divertor D_α (a.u.)
658
660
662
664
Time (ms)

Fig. 1

Case 0: no MARFE; t = 0.326662 s **Case 6: stable at top; t = 0.676685 s**

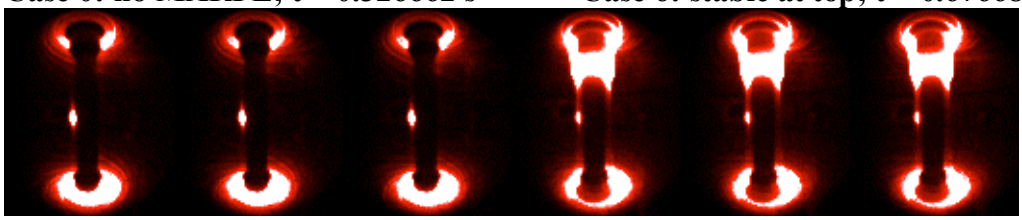

Case 1: MARFE birth; t = 0.726662 s

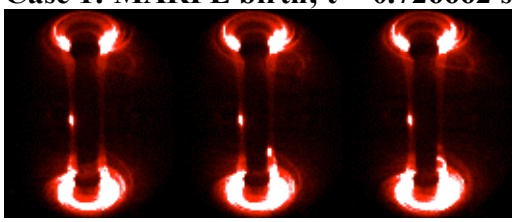

Case 2: move up; t = 0.376685 s

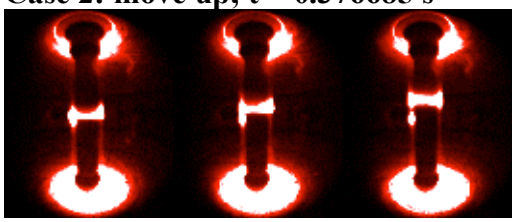

Case 3: stagnation; t = 0.493322 s

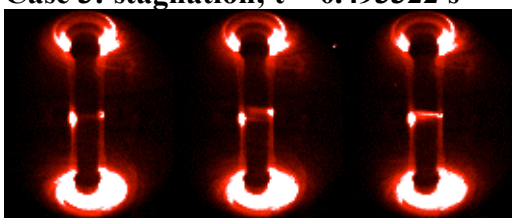

Case 4: move down; t = 0.660002 s

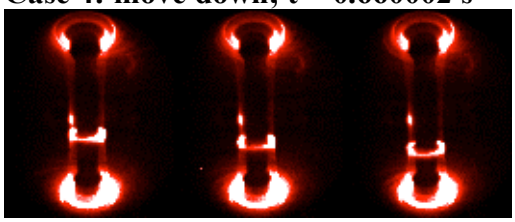

Case 5: burn; t = 0.626662 s

Fig. 2

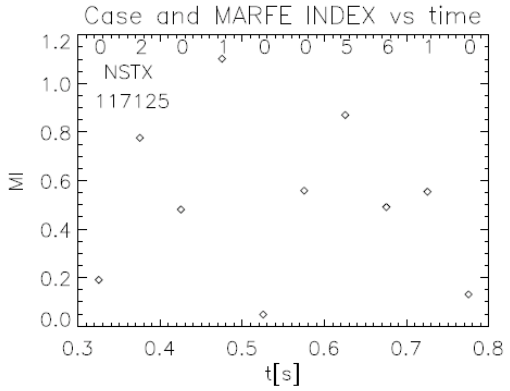
Case and MARFE INDEX vs time
0 2 0 1 0 0 5 6 1 0
NSTX
117125
MI
1.2
1.0
0.8
0.6
0.4
0.2
0.0
0.3
0.4
0.5
0.6
0.7
0.8
t[s]

Fig. 3